Incorporation of Transition Metal Ions in Aluminophosphate Molecular Sieves with AST Structure

6 AUTHORS, INCLUDING:

Pascal Van Der Voort
Ghent University
227 PUBLICATIONS **3,972** CITATIONS

SEE PROFILE

Etienne Frans. Vansant
University of Antwerp
353 PUBLICATIONS **7,253** CITATIONS

SEE PROFILE

Robert A Schoonheydt
University of Leuven
307 PUBLICATIONS **9,026** CITATIONS

SEE PROFILE

Bert M Weckhuysen
Utrecht University
594 PUBLICATIONS **16,362** CITATIONS

SEE PROFILE

ARTICLES

Incorporation of Transition Metal Ions in Aluminophosphate Molecular Sieves with AST Structure

**Ligia Frunza,[†,‡] Josephina Pelgrims,[†] Hugo Leeman,[†] Pascal Van Der Voort,[§]
Etienne F. Vansant,[§] Robert A. Schoonheydt,[†] and Bert M. Weckhuysen*[,†,⊥]**

*Centrum voor Oppervlaktechemie en Katalyse, Departement Interfasechemie, K.U. Leuven,
Kardinaal Mercierlaan 92, 3001 Heverlee, Belgium; Laboratorium voor Anorganische Scheikunde,
Departement Scheikunde, U.I. Antwerpen, Universiteitsplein 1, 2610 Wilrijk, Belgium; and
Departement Anorganische Chemie en Katalyse, Debye Instituut, Universiteit Utrecht,
Sorbonnelaan 16, P.O. Box 80083, 3508 TB Utrecht, The Netherlands*

Received: July 5, 2000; In Final Form: November 5, 2000

Transition metal ion containing aluminophosphate molecular sieves with $AlPO_4$-16 (AST) structure have been synthesized using the classic template, quinuclidine, and the corresponding salts of V^{4+}, Co^{2+}, Cr^{3+}, and Mn^{2+}. The cubic AST form was the main product, but in the presence of fluoride ions, the tetragonal AST form could also be obtained. The AST materials were characterized with X-ray diffraction, thermal analysis, scanning electron microscopy, electron spin resonance, infrared spectroscopy, and diffuse reflectance spectroscopy in the UV−vis−NIR region. Spectroscopic measurements showed that small amounts of Co^{2+} and Mn^{2+} can be incorporated in the framework. The diffuse reflectance spectra are indicative for the presence of two types of Co^{2+}, most probably taking the two framework positions T_1 and T_2 with a T_1:T_2 occupation ratio of 3−8. In contrast, V^{4+} is present in defect sites by coordination to two (or three) framework oxygen atoms. The incorporation of Cr^{3+} in the AST framework is also uncertain and two surface Cr^{3+} species were observed: clusters similar to the bulk Cr_2O_3 oxide and isolated Cr^{3+} ions in strongly distorted octahedral coordination. These spectroscopic observations were confirmed by thermal analysis results, which showed that the degree of metal ion incorporation is inversely proportional with the phase transition temperature of AST to berlinite. Furthermore, Co^{2+} and V^{4+} are very stable in the AST structure and difficult to oxidize upon heating.

Introduction

The incorporation of transition metal ions in microporous crystalline aluminophosphates ($AlPO_4$-*n*) is a challenging topic because of the potential use of these materials as heterogeneous catalysts in chemical industries.[1,2] The transition metal ions can be either incorporated in true framework sites, anchored to the framework in defect sites, or present as isolated/clustered extraframework cations.[3,4] Different coordination environments may be simultaneously found for the same metal ion, making the discrimination between these coordination environments rather involved.[4] It has been shown that Co^{2+} ions can be incorporated in the framework of many microporous aluminophosphate molecular sieves.[3,5] Indeed, spectroscopy was able to proof that tetrahedral Co^{2+} substitutes for framework Al^{3+}, although extraframework Co^{2+} is often present in these materials too. Several MnAPO-*n* molecular sieves can also be synthe-

sized,[6−14] and part of the Mn^{2+} is present in framework positions, as evidenced by, for example, high field ^{31}P ENDOR.[15] In contrast, although some data suggest the incorporation of Cr^{3+} into the framework positions of microporous aluminophosphates,[16−19] up to now there was no clear spectroscopic evidence for the isomorphous substitution of Cr^{3+}.[20−24] In the case of V^{4+} ions, it was established that V^{4+} is present in defect sites by coordination with two framework oxygen atoms.[3,4,25]

An interesting but almost unstudied microporous aluminophosphate is $AlPO_4$-16 with the AST structure. This material possesses no real channels and can be present in either the cubic or tetragonal form. The interesting feature of this molecular sieve is that it has two distinct tetrahedral framework sites with a distribution ratio of 4:1 for framework sites T_1 and T_2, and one of the key questions is if transition metal ions show during hydrothermal synthesis any preference for one of these framework sites or not. There is patent literature claiming that Co^{2+}, Cr^{3+}, Mn^{2+}, and V^{4+} ions can occupy framework positions in the AST structure,[29−32] but research papers dealing with the characterization of these materials are very scarce.[33,34] Here, we report on the hydrothermal synthesis and the characterization of CoAPO-16, MnAPO-16, CrAPO-16, and VAPO-16 molec-

* To whom the correspondence should be addressed. E-mail:
bert.weckhuysen@agr.kuleuven.ac.be.
† K.U. Leuven.
‡ On leave from the National Institute of Materials Physics, PO Box Mg
07, R-76900 Bucharest-Magurele, Romania.
§ U.I. Antwerpen.
⊥ Universiteit Utrecht.

ular sieves. The aim of this study was to distinguish framework and extraframework metal ion species, to monitor changes in the oxidation state of the metal ions during heating, and to study the thermal stability of the AST molecular sieves. The techniques used are X-ray diffraction (XRD), thermal analysis (TGA-DTA), scanning electron microscopy (SEM), Fourier Transform infrared spectroscopy (FTIR), diffuse reflectance spectroscopy in the UV−vis−NIR region (DRS), and electron spin resonance (ESR).

Experimental Section

1. Hydrothermal Synthesis. The cubic AST materials (C) were hydrothermally synthesized from reaction gels with a molar composition of $(1-x)Al_2O_3-P_2O_5-2xM-0.5Q-0.5TPA-30H_2O$ where Q is quinuclidine, TPA is tripropylamine, and M represents the corresponding metal ion. In the case of Mn and Cr, $x = 0.02$, but series of samples with different concentrations of Co and V were also made starting from gels with $x = 0.005$, 0.01, 0.02, 0.04, and 0.08. The gels were prepared as previously reported[26,35] for $AlPO_4$-16 with the difference that the metal salts were added to the aluminum sol before the aqueous solution of the template was admixed and that the amount of Q was decreased to half by using TPA as cotemplate. The homogenized gels were treated thermally at the desired temperature under static conditions in Teflon-lined autoclaves. Afterward, the autoclaves were cooled, and the resulting solids were decanted, washed several times with bidistilled water, and dried overnight at 333 K. To obtain the tetragonal AST materials (T), HF was introduced[27] after adding Q, and TPA was then dropwise added till a pH of 6.5 was reached. The samples made were labeled as M_xAPO-16(X) with x the amount of the transition metal ion in the gel and X the form of the AST material (C or T). The following reactants were used as received: Q (Acros, p.a.), pseudoboehmite (Catapal, Condea), 85 wt % H_3PO_4 (Janssen, p.a.), TPA (Janssen, p.a.), $VOSO_4\cdot5H_2O$ (Merck, p.a.), $Co(CH_3COO)_2\cdot4H_2O$ (Acros, p.a.), $MnSO_4\cdot H_2O$ (Merck, p.a.), $CrCl_3\cdot6H_2O$ (UCB, p.a.), and HF (AnalaR, 40%).

2. Sample Characterization. XRD powder patterns were obtained using a Siemens D5000 diffractometer with Cu Kα radiation. The overall crystallinity has been estimated either from the intensity of the highest diffraction peak of each individual crystalline phase or as the sum of the intensities of the five highest peaks. ESR spectra were recorded at 150 and/or 300 K with a Bruker ESP300E spectrometer at X-band. The ESR spectra of V^{4+}-containing materials were simulated with the SIMPOW program of Nilges,[36] whereas for Cr^{3+} or Mn^{2+} the PIP program[37] was used. SEM was performed with a Phillips 515 microscope on samples deposited onto an alumina support and coated with a gold film. TGA−DTA measurements were carried out using a Setaram TG-DTA92 apparatus in a helium/oxygen flow with a heating rate of 5 K/min. FTIR spectra were recorded with a Nicolet 750 FTIR apparatus, in the range 400−4000 cm^{-1}. The KBr technique was used to study the framework vibrations, whereas wafers were used to measure the removal of water and template molecules from the as-synthesized materials. DRS spectra were recorded with a Varian Cary 5 spectrometer against a Halon white standard either in air at room temperature or in a special cell with a sidearm for recording ESR spectra. Reflectance data were converted to absorption spectra using the Kubelka−Munk function $F(R_\infty)$, allowing for the quantitation of the species responsible for the absorption bands. The spectra were deconvoluted into Gaussian components using the Microcal Origin 5.0 software.

3. Sample Pretreatment. To check the thermal stability of the as-synthesized materials, the samples were submitted to a

TABLE 1: Synthesis Conditions Leading to the Formation of AST Molecular Sieves

sample	M/P[a]	Q/P	TPA/P	temp (K)	time (h)	XRD phases[b]
$V_{0.01}APO$-16(C)	0.01	0.22	0.22	448	72	AST-C
$V_{0.01}APO$-16(T)	0.01	0.25	0.67	453	120	AST-T
$Co_{0.01}APO$-16(C)	0.01	0.22	0.22	448	72	AST-C + [AFI]
$Co_{0.01}APO$-16(T)	0.01	0.22	0.90	448	130	AST-T + [AWW] + [AFI]
$Mn_{0.01}APO$-16(C)	0.01	0.30	0.50	453	48	AST-C
$Cr_{0.01}APO$-16(C)	0.01	0.25	0.50	453	48	AST-C

[a] The metal content in the solids after hydrothermal synthesis are very close to those in the initial synthesis gel. [b] Brackets symbolize that there are traces of the corresponding phase(s).
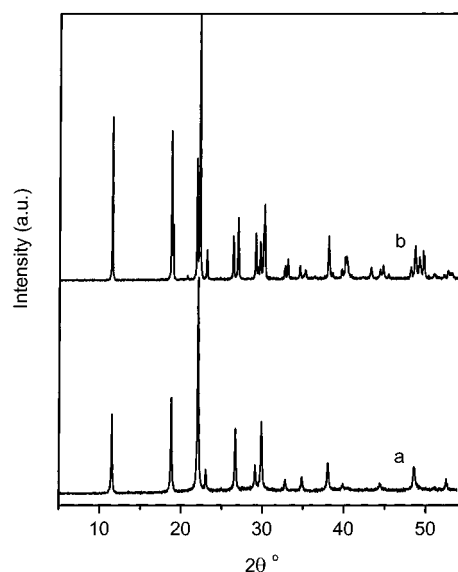

Figure 1. XRD powder patterns of molecular sieves in the as-synthesized form: (a) $V_{0.01}APO$-16(C) and (b) $V_{0.01}APO$-16(T).

thermal treatment in air up to 873 K in steps of 100 K for 10 h at each temperature. After each step, the samples were analyzed with XRD, DRS, and ESR. FTIR measurements were done on self-supported wafers treated in helium or oxygen at temperatures up to 723 K in a quartz cell with IR transparent windows, which was attached to a conventional flow/vacuum line. A specially designed DRS-ESR cell also allowed treatments under controlled temperature and atmosphere. The powders were first granulated with a mean size of 0.25−0.40 mm. The samples were either dehydrated under vacuum or in a helium flow, treated in oxygen, or reduced in a flow of hydrogen. ESR and DRS spectra were collected after each treatment step. Leaching experiments with solutions of ammonium acetate, known to eliminate vanadium polymeric surface species,[38] were performed for samples containing vanadium and the ESR spectra were recorded afterward.

Results and Discussion

1. Phase Purity and Crystal Morphology. Typical examples of synthesis conditions leading to pure M_xAPO-16 materials are reported in Table 1, while two representative XRD patterns of as-synthesized samples are presented in Figure 1. The pure C form was obtained when using the recipe of Wilson et al.,[26,35] whereas the T form was formed in the presence of F$^-$ ions.[27,28] The as-synthesized AST samples have a high crystallinity, although some of the materials contain traces of additional phases such as $AlPO_4$-22 (AWW structure) and $AlPO_4$-5 (AFI structure), which are known to be formed with Q or TPA as

Transition Metal Ions in Molecular Sieves
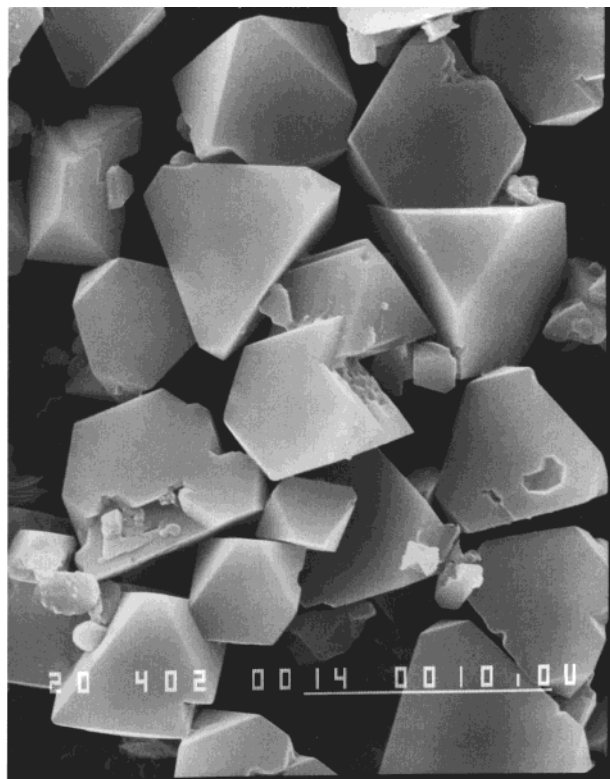
J. Phys. Chem. B, Vol. 105, No. 14, 2001 **2679**

Figure 2. SEM picture of $V_{0.01}APO-16(T)$.

Figure 3. Variation of the crystallinity degree of the $M_{0.01}APO-16(C)$ samples due to a heating treatment overnight at specified temperatures: V (▼), Cr (●), Co (▲), and Mn (■).

template. Dense phases such as tridymite or berlinite may also appear during the hydrothermal synthesis. SEM analysis shows that the as-synthesized materials are composed of aggregates with the external habitus of the already known[27,28,39] tetrahedral shape (not shown for brevity). However, the samples of the T form do not possess only tetrahedrally shaped crystals but also octahedral ones, as illustrated in Figure 2. The dimensions of the aggregates were usually between 1 and 15 μm.

The AST clathrate preserves the template, at least partially, even after calcination at 773 K, but according to the XRD patterns, the structure starts to break down, depending on the calcination parameters, i.e., temperature and time. Figure 3 illustrates the transformation of the AST structure into amorphous material in the case of the $M_{0.01}APO-16(C)$ samples. The relative crystallinity degree was estimated as the ratio of the sum of the intensities of the five highest XRD peaks of the sample calcined overnight at different temperatures and of the as-synthesized sample. Taking into account the similar metal loading of the as-synthesized samples, it can be concluded that the thermal stability of these AST materials depends on the nature of the metal ion, decreasing in the order V > Mn > Cr > Co. A similar decrease of the thermal stability of the ATO or AEL framework due to the incorporation of metal ions has been reported for Zn, Mg, Mn, Cr, Ni, and Cd.[11,40]

2. Thermal Analysis. TGA–DTA of the as-synthesized materials was performed in a continuous flow of a mixture of helium and oxygen. Obviously, the calcination process proceeds in several stages, and the DTA curves are presented in Figure 4. A comparable thermal behavior has been reported for $AlPO_4$-16 and for other metal-substituted AlPO-*n* materials.[40] After desorption of water up to ca. 400 K, the further stages reflect an endothermic desorption and decomposition of the template and especially the exothermic oxidation of the template. The DTA peaks of the $Cr_{0.01}APO-16$ sample are overlapping in a broad feature ranging from 700 to 1200 K. This feature became more structured in the case of $Co_{0.01}APO-16(C)$ and $Mn_{0.01}$-
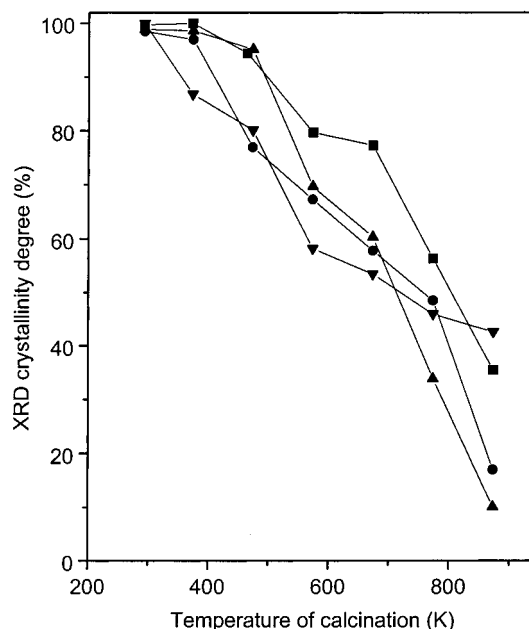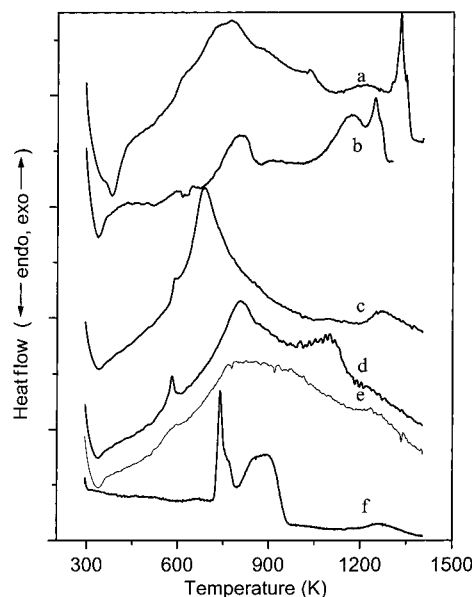

Figure 4. DTA curves of as-synthesized materials: (a) AlPO-16(C), (b) $Mn_{0.01}APO-16(C)$, (c) $V_{0.01}APO-16(C)$, (d) $Co_{0.01}APO-16(C)$, (e) $Cr_{0.01}APO-16(C)$, and (f) $V_{0.01}APO-16(T)$.

APO-16(C), whereas the $V_{0.01}APO-16(T)$ sample exhibits clear, sharp peaks, indicating a well-defined guest−host interaction of the template within the molecular sieve framework.

A small amount of the protonated template might exist also in the case of C forms of the metal-modified aluminophosphate AST materials as a result of the (partial) substitution of divalent transition metal ions in the framework positions. Thus, the most important peak in the DTA curve appears at 750 K for $AlPO_4$-16 and at 770 K for MnAPO-16 and CoAPO-16. This peak is ascribed to the template interaction with the acid sites of the molecular sieve.[11,40,41] Up to 1000 K, the DTA curve of CrAPO-16 is shaped almost similarly to the binary $AlPO_4$-16 material. In addition, protonated template molecules are more abundant in the $V_{0.01}APO-16(T)$ sample than in the $V_{0.01}APO-16(C)$ sample, in order to compensate for the fluoride ions present.

**TABLE 2: Water and Template Molecules in One Unit Cell of As-Synthesized MAPO-16**

sample	water molecules per uc	template molecules per uc
AlPO-16(C)	5.2	2.2
$V_{0.01}$APO-16(C)	9.9	4.3
$V_{0.01}$APO-16(T)	0.2	4.0
$Cr_{0.01}$APO-16(C)	5.5	2.6
$Co_{0.01}$APO-16(C)	6.4	2.6
$Mn_{0.01}$APO-16(C)	6.0	2.7

At high temperatures, a phase transition takes place to the berlinite structure, which is known to be the most stable form of aluminophosphates. The peak corresponding to this phase transition shifts from 1261 to 1311 K, in the case of $AlPO_4$-16(C), to 1263 K for $Cr_{0.01}$APO-16(C), to 1248 K for $V_{0.01}$-APO-16(C), to 1147 K for $Mn_{0.01}$APO-16(C), and to 1098 K for $Co_{0.01}$APO-16(C). Taking into account the similar metal ion loading of these materials, this phase transition temperature can be taken as a criterion for the introduction of framework stress due to the incorporation of transition metal ions in the framework. Thus, the stability of the framework seems to decrease in the order V > Cr > Mn > Co. This suggests already that the V^{4+} and Cr^{3+} ions are not really incorporated in the $AlPO_4$-16 structure.

Table 2 summarizes the amounts of water and template present in a unit cell (uc) of the materials as estimated by TGA−DTA. Thus, the water content is low and ranges from 5 to 10 wt %, whereas Schott-Darie et al.[27] and Schreyeck et al.[28] found about 3−8 wt % in their AlPO materials. At the same time, the mass loss during the high temperature heating, namely between 550 and 900 K, ranges from 8 to 16 wt %, corresponding to 2.2−4.3 template molecules per uc. According to the literature, the number of the template molecules per uc has to be close to 4, which corresponds to the presence of one Q molecule in each octadecahedral cage.[27,28] Our samples contain less template molecule per main cage, but it is also clear that the structure is still very stable. In addition, the TGA−DTA data show that within the experimental errors, the template content as well as the water content does not directly correlate with the nature or with the loading of the transition metal ions in these molecular sieves.

3. IR Spectroscopy. Typical IR spectra of the $M_{0.01}$APO-16 samples obtained by the KBr technique are given in Figure 5. The spectra consist of rather sharp absorptions, confirming the high crystallinity of the samples. Three regions[42,43] are important: (1) the 940−1200 cm^{-1} region features the stretching vibrations of T−O−T and T−O−M, where T stands for the central atom in the primary units as TO_4 tetrahedra; (2) the 750−950 cm^{-1} region, in which the bending of X−OH (X = any atom other than O and H) occurs; and (3) the region <600 cm^{-1}, where the bending vibrations of T−O−T and T−O−M appear. The most intense are the peaks due to the asymmetric stretching vibrations of the T−O−T groups, but they consist of a composite envelope of overlapping peaks.

For a given crystalline AST material, the spectra are similar for all the samples containing the above-mentioned transition metal ions, as well as for the binary $AlPO_4$-16 sample, since there are no marked differences in the IR bands associated with the vibrations of the $AlPO_4$-16 lattice. The resemblance with the spectrum of pure $AlPO_4$-16 suggests a rather small distortion of the lattice caused by the incorporation of the transition metal ions. However, the T form shows more bands in regions 2 and 3 than the C form due to a lowering of the framework symmetry. At the same time, the spectra in Figure 5 provide evidence for
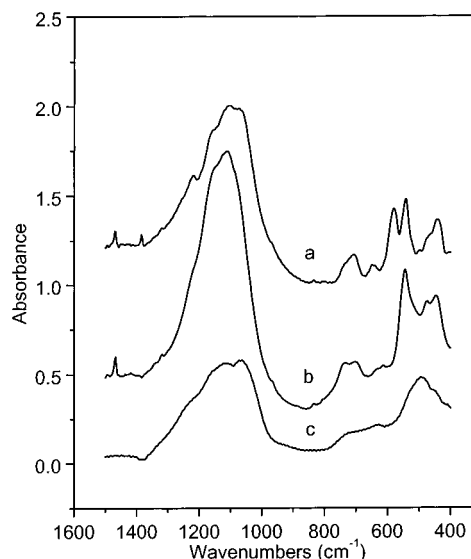
Figure 5. FTIR spectra in KBr pellets: (a) as-synthesized $V_{0.01}$APO-16(C), (b) as-synthesized $V_{0.01}$APO-16(T), and (c) calcined $V_{0.01}$APO-16(C).
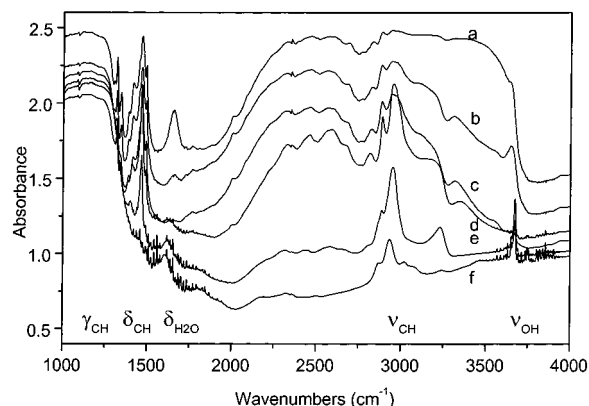
Figure 6. FTIR spectra of $V_{0.01}$APO-16(C) at the following temperatures: (a) 298 K, (b) 333 K, (c) 393 K, (d) 523 K, (e) 693 K, and (f) 773 K.

the incorporation of the template in the AST structure, as expected for clathrasil-type materials. The vibrational modes of Q encapsulated in the molecular sieves are similar to those observed in the crystalline form of the template. The spectra seem to show that most of the templating amine encaged in the framework structure is neutral. Besides, the interaction between the template and the framework induces some rigidity into the molecule, and accordingly, the vibrations corresponding to the CH_2 stretching, as well as to the bending vibrations, are shifted toward wavenumbers higher than in the solid state.

The spectrum of the calcined samples (e.g., curve c in Figure 5) confirmed the removal of (most of) the template as well as the disappearance of sharp bands of the bending vibrations, due to changes in the structure. To get more information about the OH stretching region of the MAPO-16 samples, we have performed IR experiments by collecting the spectra when the desorption temperature increases. A representative set of spectra as obtained for the $V_{0.01}$APO-16(C) sample is presented in Figure 6. The peak at 3676 cm^{-1} ascribed generally to the stretching vibration of P−OH groups[44] is observed, and these groups probably originate from defects present in the structure, although a contribution of the terminal P−OH on the external surface might be taken into consideration too. Stretching vibrations of other OH groups are difficult to observe, although the less intense peak around 3750 cm^{-1} is due to the Al−OH
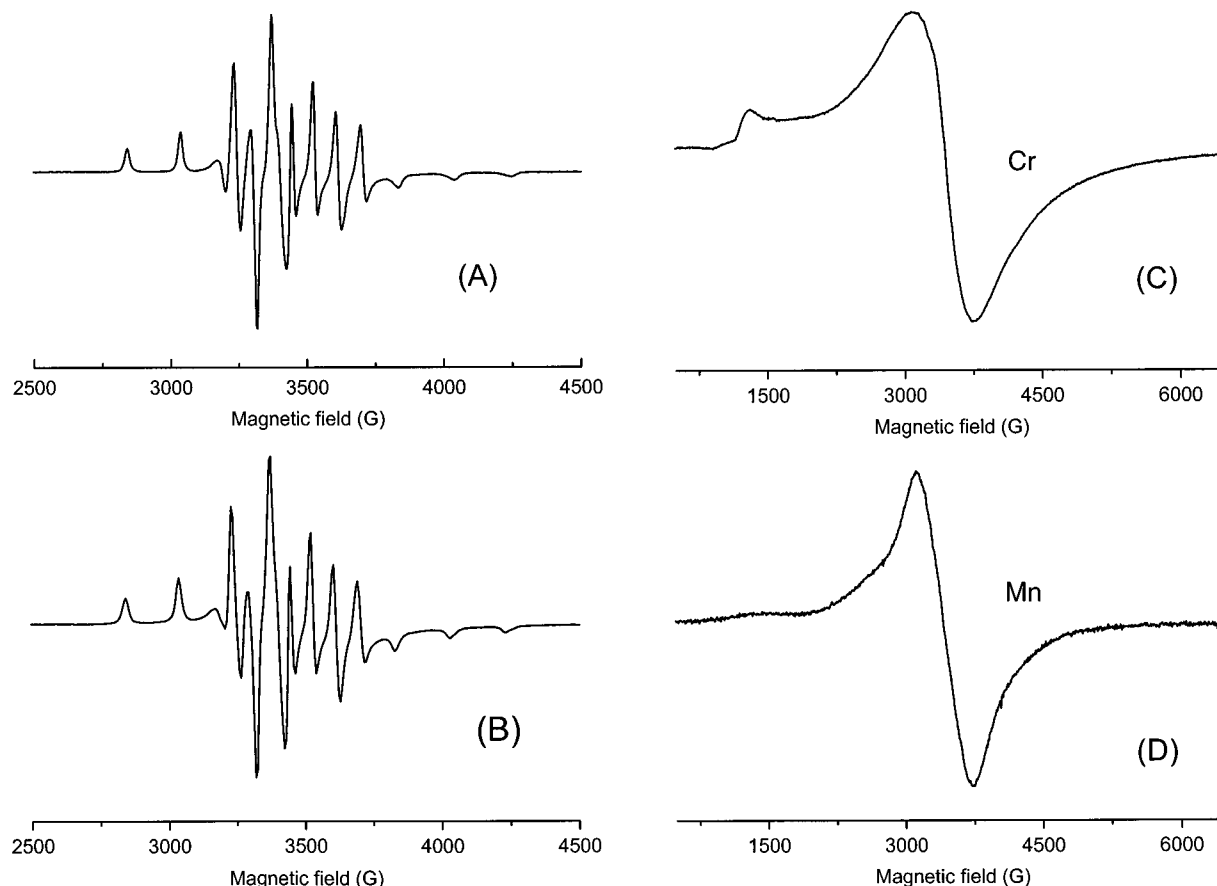
Figure 7. ESR spectra (measured at 120 K) of (A) $V_{0.01}APO$-16(C), (B) $V_{0.01}APO$-16(T), (C) $Cr_{0.01}APO$-16(C) and (D) $Mn_{0.01}APO$-16(C).

stretching vibration.[44] There are also broad, less intense peaks at a lower region (3300−3640 cm^{-1}), originating probably from the acidic hydroxyls[45−47] bridging a metal and a P atom, and around 3660 cm^{-1}, maybe due to the stretching of the OH group bound to metal cations (e.g., V−OH).[48,49] In the frequency range in which the framework itself does not absorb, the vibrations of the template molecules can be monitored. It results from Figure 6 that the CH stretching and deformation vibrations of the template are still present for the samples heated in helium at 773 K (2957 and 2897 cm^{-1} bands). The broad bands observed at 3508, 3436, and 3152 cm^{-1} correspond to combinations and overlappings of stretching and deformation vibrations of H_2O, NH_2, and CH_2 groups, whereas the sharp bands at 1635 and 1508 cm^{-1} can be assigned to the bending vibrations. The peak due to the deformation vibration of water decreases gradually with increasing temperature.

4. ESR Spectroscopy. Typical ESR spectra of as-synthesized $M_{0.01}APO$-16 samples are shown in Figure 7. The ESR spectra of the samples containing V are characteristic for well-dispersed and immobile V^{4+}-species; they have a rather horizontal baseline, indicating that there are no polynuclear vanadium oxide species present. The corresponding g and A values were obtained by simulating the ESR spectra and considering a rhombic symmetry for the vanadium species, as was proposed for VAPO-5 aluminophosphate molecular sieves.[50] These values are given in Table 3 and are in good agreement with the values given in the literature for the vanadyl VO^{2+} species either in aqueous solutions or in other VAPO-n structures. We can deduce from these ESR parameters and the empirical correlation diagram of Davidson and Che[60] that the oxygen coordination around the V^{4+} ion is octahedral or square-pyramidal.

It is important to notice that the two forms of the VAPO-16 material have almost identical ESR spectra (Figure 7), and as a

consequence, similar ESR parameters were obtained by simulation. This means that the local symmetry of the vanadium ion has to be rather similar in all these samples, even though it is present in different forms. In other words, the similarity of the local geometry of V^{4+} might be another indication that this metal ion is not entering into a true framework position with tetrahedral symmetry. However, the anchoring at the framework is rather strong, as shown by leaching experiments as well as by long duration calcination treatments. Thus, leaching experiments do not really affect the intensity of the ESR signals, while upon calcination, the vanadium-containing samples exhibit ESR spectra with lower intensity, due to the oxidation of V^{4+} to the ESR-silent V^{5+} species. The integrated intensity of the V^{4+} signals, however, decreased only to 35−60% in the case of the AST samples calcined overnight in air but to 10% or less in the case of other materials having AEL, AFO, or AFI structure and to 0% for amorphous VAPO materials.

The ESR spectra of VAPO-16 materials were also used to estimate the V content. The variation of the number of vanadyl spins, as measured by double integration of the ESR spectrum, is given in Figure 8 as a function of the V amount offered to the synthesis gel. It results that there is a rather good linear relationship, indicating a gradual incorporation of the V^{4+} ions in the corresponding molecular sieves. Besides, the linear relationship indicates that the amount offered does not reach a maximum value in the case of VAPO-16 molecular sieves, as was observed for VAPO-11,[38] at least for the amounts studied in this paper.

Two distinct signals are present in the ESR spectrum of the CrAPO-16 molecular sieves (Figure 7). One ESR signal is large and broad, centered at around $g = 2.0$; the other is also broad but appears at $g_{eff} = 4.12$. Similar signals were also reported for CrAPO-5 sieves;[54] they were ascribed to Cr^{3+} ions with

TABLE 3: ESR Parameters of As-Synthesized MAPO-16 Molecular Sieves and of Some Reference Compounds[a]

sample	g_{xx}	g_{yy}	g_{zz}	A_{xx} (G)	A_{yy} (G)	A_{zz} (G)	w_{xx} (G)	w_{yy} (G)	w_{zz} (G)	D (G)	E (G)	assignment	reference
$V_{0.01}$APO-16(C)	1.983	1.974	1.933	71.6	72.4	199.1	15	15	15	−	−	isolated distorted octah VO^{2+}	this work
$V_{0.01}$APO-16(T)	1.985	1.974	1.934	71.0	69.4	199.4	15	15	15	−	−	isolated distorted octah VO^{2+}	this work
VAPO-5	1.993	1.977	1.947	74.2	74.2	196.0				−	−	isolated distorted octah V^{4+}	50
VAPO-5	1.983	1.983	1.932	78	78	198						octah VO^{2+}	51
VAPO-5	1.976	1.976	1.935	71	71	196						isolated distorted octah V^{4+}	52
VAPO-11	1.983	1.974	1.935	74.8	66.4	197.4	25	25	25			isolated distorted octah VO^{2+}	38
VAPO-17	nr	nr	1.933			199.2						isolated octah VO^{2+}	53
VAPO-41	1.985	1.971	1.935	73.4	69.6	196.2	25	25	25	−	−	isolated distorted octah V^{4+}	38
$Cr_{0.01}$APO-16(C)	1.998	1.998	1.998	−	−	−	600	600	600	0	0	Cr_2O_3-like	this work
	1.990	1.900	1.900				900	500	500	4750	1600	isolated highly distorted Cr^{3+}	
CrAPO-5	1.987	1.987	1.987	−	−	−	556	556	556	0	0	Cr_2O_3-like	54
	1.987	1.865	1.865				800	400	400	5358	1790	isolated highly distorted Cr^{3+}	
CrAPSO-5	1.98	1.98	1.98				500	500	500	5409	1803	distorted octah Cr^{3+}	55
	4.00	4.00	2.00									tetrah Cr^{3+}	
CrMCM-41	2.05	nr	nr										56
$Mn_{0.01}$APO-16(C)	2.00	2.00	2.00	90	90	90	30	30	30	140	0	octah Mn^{2+}	this work
	1.980	1.980	1.900				800	600	600			tetrah Mn^{2+}	
MnAPO-5				90	90	90	25	25	25	140	0	distorted octah	8
MnAPO-5	2.0			91								extraframework octah Mn^{2+}	14
	4.3											distorted tetrah framework Mn^{2+}	
MnAPO-11	2.01	2.01	2.01	87.7	87.7	87.7						axially symmetric Mn^{2+}	9
MnAPO-11	2.004	2.004	2.004	90	90	90	50	50	50			isolated octah Mn^{2+}	12
	2.004	2.004	2.004	85.4	85.4	85.4	500	500	500			interacting Mn^{2+}	
	4.27	2.42	1.47									isolated distorted tetrah Mn^{2+}	
MnAPO-36	1.99	nr	nr	89								probably framework Mn^{2+} in distorted tetrah symmetry	57
MnMCM-41	2.007	2.007	2.007	97	97	97	12	12	12			distorted octah Mn^{2+}	58
	5.2	3.2		43			214					distorted tetrah extraframework Mn^{2+}	
	2.004											framework tetrah Mn^{2+}	
MnA	2.001			106						424		distorted octah Mn^{2+}	59
	−			96.5						0		tetrah Mn^{2+}	

[a] nr = not reported.

octahedral symmetry in Cr_2O_3-like clusters and to isolated, magnetically well-dispersed Cr^{3+} species. The first signal shows the presence of strongly interacting extraframework Cr^{3+} species, whereas the second one is due to isolated Cr^{3+} species, situated in extraframework positions, namely at the surface of the molecular sieve. The corresponding ESR parameters are given in Table 3 and are in agreement with those of related materials.

The ESR spectrum of the as-synthesized MnAPO-16(C) sample shows an intense and large signal at $g_{eff} = 2$ and a very broad and weak line at $g_{eff} = 4.2$. It is similar to those observed for Mn^{2+} ions in a wide variety of oxide materials and molecular sieves[6–14,16–18] that have in addition a rather high content of Mn^{2+} ions. Thus, the signal at $g = 2$ is characteristic for octahedrally coordinated Mn^{2+}, indicating a certain amount of Mn ions in extraframework positions. However, no hyperfine sextet structure, due to the hyperfine interaction with the Mn nucleus ($I = \frac{5}{2}$), as expected for the central transition $M_S = -\frac{1}{2}$ to $M_S = \frac{1}{2}$ can be detected. The other allowed transitions as well as the forbidden transitions, which can also appear due to high order effects of zero-field splitting, contribute to the background of the spectrum, leading to a poorly resolved ESR spectrum.[14] To account for the ESR signal in Figure 7, enhanced spin−spin exchange interaction between neighboring Mn^{2+} centers has to be supposed, probably via phosphate groups.[14] The corresponding Mn ions either occupy the nearby or adjacent aluminophosphate framework positions or form small clusters. On the other hand, the resonance at $g_{eff} = 4.2$ in the spectrum of MnAPO-16 might be due to tetrahedrally coordinated Mn^{2+} with strong rhombic distortion.[14] According to Kevan et al.,[58] framework substitution of Mn^{2+} is evidenced by a large isotropic signal, which also exists in our simulated spectra.

5. DRS Spectroscopy. The as-synthesized aluminophosphate molecular sieves containing V^{4+} or Cr^{3+} are green, those with Co^{2+} are blue, and those with Mn^{2+} are light pink. Accordingly, these materials exhibit absorption bands in the UV−vis region of the DRS spectrum. Typical spectra are presented in Figure 9, together with a proposed deconvolution in Gaussian components. For each series of spectra, the same number of components with the same band profile and almost the same position and bandwidth were used. The consistency of the deconvolution is an indication that the proposed deconvolution has a physical meaning, while the fact that a consistent interpretation can be given is another strong point for the proposed deconvolution. The results of the spectral deconvolution are summarized in Table 4, along with the corresponding assignments made by considering the absorption bands of several reference compounds. It is important to stress that the DRS spectra also show overtone and combination bands of the stretching/deformation of adsorbed or coordinated water and hydroxyl groups, the most intense being the one centered at 5160 cm^{-1}.

Figure 9A shows the DRS spectrum of as-synthesized VAPO-16(C) and the proposed deconvolution of the d−d region. Two transitions can be resolved, which are located at 11 300 and 14 500 cm^{-1}. These transitions are also observed for other VAPO-n molecular sieves and are assigned to pseudo-octahedral V^{4+} species anchored to the surface. The red shift of the

Transition Metal Ions in Molecular Sieves

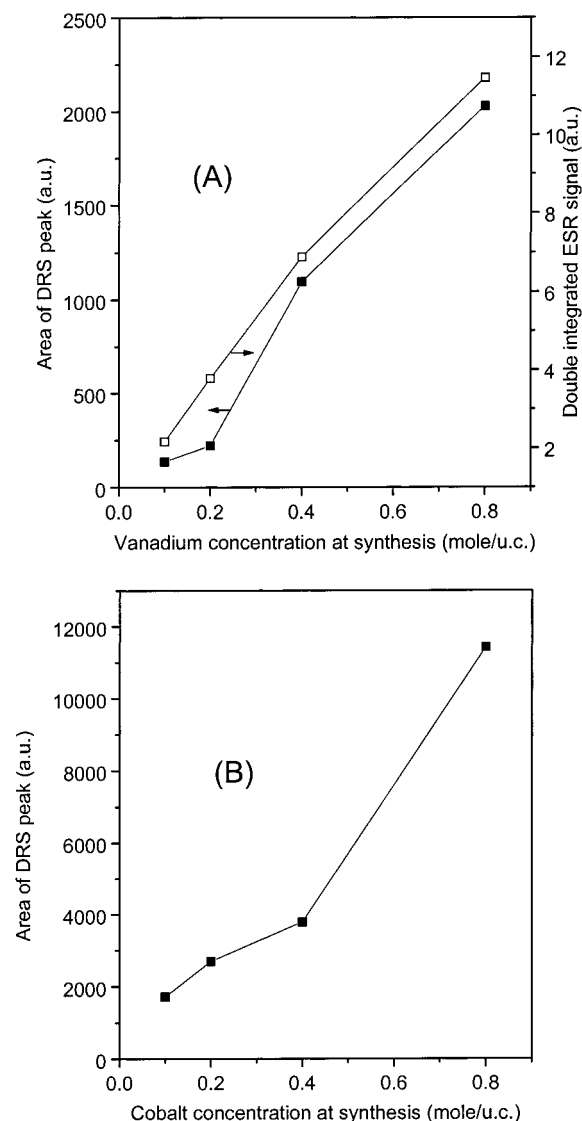*J. Phys. Chem. B, Vol. 105, No. 14, 2001* **2683**

Figure 8. Incorporation of (A) V^{4+} and (B) Co^{2+} in M_xAPO-16(C): DRS and ESR intensity as a function of the metal content (x) in the synthesis gel.

absorption bands in comparison with VAPO-5 and VAPO-11 could be due to a change in the coordination environment of V^{4+}. More specifically, it could be due to an increasing number of framework oxygen atoms around V^{4+}. Although there are to the best of our knowledge no studies about the position of framework oxygen atoms of microporous aluminophosphates in the spectrochemical series, we believe that the ligand field strength of a framework oxygen is lower than that of a water molecule. Taking into account the rule of the average environment[68] (the decrease of the crystal field strength upon substitution of water by framework oxygen atoms is a linear function of the number of oxygen ligands), one can conclude that V^{4+} ions in VAPO-16 are surrounded by more framework oxygen atoms than in the AEL and AFI structures.

All the Co-containing AST aluminophosphate molecular sieves, regardless of the form, possess two overlapping triplet structures (Figure 9B), which can be resolved in two sets of three Gaussian bands by spectrum deconvolution. The resolved Gaussian bands are included in Figure 9B, while Table 4 summarizes the positions of the individual Gaussian bands. There is also an absorption band present at around 20 000 cm^{-1}, which is due to the presence of octahedrally coordinated nonframework Co^{2+}. The two sets of Gaussian bands can be

explained in terms of two tetrahedral Co^{2+} species with a different local coordination environment. Indeed, it is known that the triplet absorption band is sensitive to the degree of deviation from the tetrahedral symmetry of Co^{2+} and most probably each triplet of Co^{2+} is then due to the two distinct tetrahedral framework sites, T_1 and T_2, of the AST structure in either the cubic and tetragonal form. The ratio of the intensity of the Co^{2+} (T_1) triplet over the intensity of the Co^{2+} (T_2) triplet is in the range of $3.5-8$ for the samples with different Co loading and form. This value is obtained by assuming similar extinction coefficients for both framework sites. It is not far from the $T_1:T_2$ distribution ratio of 4 in the AST structure, suggesting that there is no preference of Co^{2+} for one of the two framework sites during hydrothermal synthesis. The observation of two distinct framework Co^{2+} species in microporous crystalline aluminophosphates has only been proposed in the past for the CHA structure[69] and is surprising given the fact that many AlPO$_4$-n structures have more than one T site. Possible explanations are the preference of Co^{2+} for one of these T sites or the similarity between the coordination environment of these T sites. In both cases, it was impossible up to now to distinguish them by spectroscopy. At this stage of the investigations we cannot assign yet the two observed triplet structures to Co^{2+} species having a specific local symmetry in the AST structure. Further studies, both experimental and theoretical, are necessary to find out why the AST structure better shows these spectroscopic differences between T sites than other structures.

Figure 9C shows the DRS spectrum of $Cr_{0.01}APO$-16(C), and spectral deconvolution resolves two main absorption bands at 15 735 and 22 380 cm^{-1}, which are due to pseudo-octahedrally coordinated Cr^{3+}. Similar bands were observed for CrAPO-5 materials, and the red shift of the first allowed d−d transition of CrAPO-16 when comparing with the spectrum of $Cr(H_2O)_6^{3+}$ complex can be explained in terms of an increasing number of framework oxygen atoms surrounding the Cr^{3+} site. The DRS spectrum of $Mn_{0.01}APO$-16(C) is given in Figure 9D, and two distinct Mn^{2+} ions in a distorted octahedral and tetrahedral coordination can be observed. The assignment of the absorption bands to the octahedral extraframework Mn^{2+} species is straightforward, while the assignment of the second Mn^{2+} species is only tentative.

The DRS spectra were also used to quantify the amount of the transition metal ion in the as-synthesized AST materials by integrating the intensity (in Kubelka−Munk units) in the frequency region of (a) certain absorption band(s). It can be seen in Figure 8 that the intensity of the d−d transitions of Co^{2+} and V^{4+} more or less linearly increases with increasing metal loading. To get more information on the local geometry of the Co^{2+} sites, the as-synthesized CoAPO-16 materials were dehydrated overnight at 393 K, subsequently calcined in an oxygen flow at 800 K, and then reduced in a hydrogen flow at 623 K. Figure 10 shows the changes taking place after each treatment step for a $Co_{0.02}APO$-16(C) sample. The color changes from blue to yellow-green upon calcination, and consequently, the intensity of the triplet bands in the visible region decreases while the one in the near-infrared broadens. In addition, a new and intense band appears at around 30 000 cm^{-1}. Despite this intensity increase of absorption bands in the ultraviolet region associated with the oxidation of part of the Co^{2+} ions, the intensity of the triplet in the visible region decreases only with 15%. This indicates that most of the Co^{2+} ions remain in the divalent state after calcination. In addition, there are some red shifts of the triplet in the visible region by dehydration,
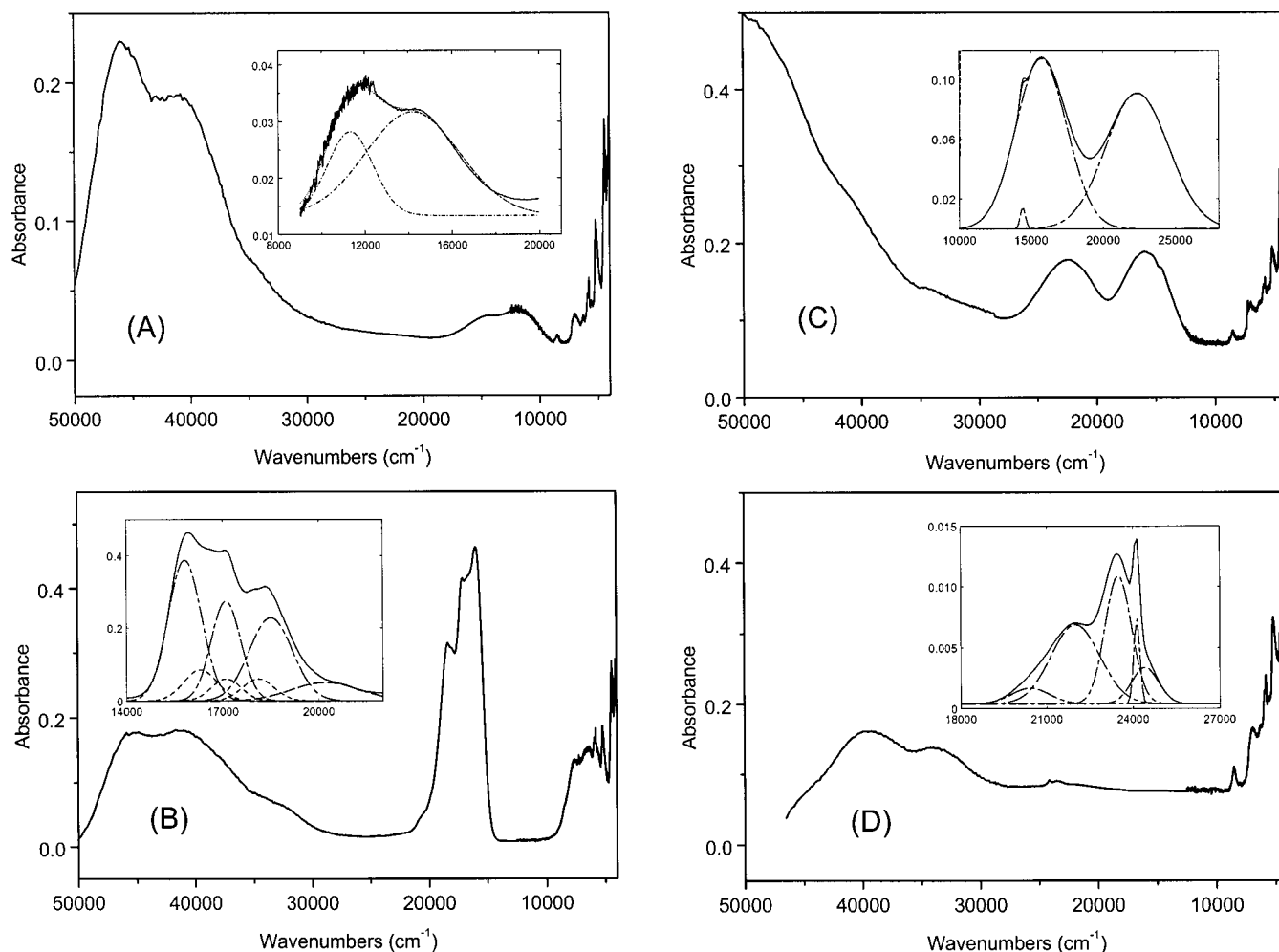
Figure 9. DRS spectra of as-synthesized aluminophosphate materials: (A) $V_{0.01}APO\text{-}16(C)$, (B) $Co_{0.01}APO\text{-}16(C)$, (C) $Cr_{0.01}APO\text{-}16(C)$, and (D) $Mn_{0.01}APO\text{-}16(C)$. The insert shows the corresponding deconvolution in Gaussian components.

TABLE 4: Absorption Bands in the Visible Range of As-Synthesized MAPO-16 and of Some Reference Compounds

sample	positions (cm^{-1}) and assignments	reference
$V_{0.005}APO\text{-}16(C)$	11 300 ($^2B_{2g} \rightarrow {}^2E_g$); 14 500 ($^2B_{2g} \rightarrow {}^2B_{1g}$)	this work
VAPO-5	131 00 ($^2B_{2g} \rightarrow {}^2E_g$); 16 500 ($^2B_{2g} \rightarrow {}^2B_{1g}$)	50
VAPO-11	13 500 ($^2B_{2g} \rightarrow {}^2E_g$); 16 500 ($^2B_{2g} \rightarrow {}^2B_{1g}$)	38
$VO(H_2O)_5{}^{2+}$	13 000 ($^2B_{2g} \rightarrow {}^2E_g$); 15 900 ($^2B_{2g} \rightarrow {}^2B_{1g}$)	61
$Co_{0.01}APO\text{-}16(C)$	15 900; 17 150; 18 500 ($^4A_2(F) \rightarrow {}^4T_1(P)$ triplet I); 15 600; 16 670; 18 170 ($^4A_2(F) \rightarrow {}^4T_1(P)$ triplet II); 20 200 ($^4T_{1g}(F) \rightarrow {}^4T_{2g}(F)$)	this work
$Co_{0.01}APO\text{-}16(T)$	15 700; 17 050; 18 500 ($^4A_2(F) \rightarrow {}^4T_1(P)$ triplet I); 14 900; 16 430; 18 000 ($^4A_2(F) \rightarrow {}^4T_1(P)$ triplet II); 20 200 ($^4T_{1g}(F) \rightarrow {}^4T_{2g}(F)$)	this work
CoAPO-16	15 970; 17 240; 18 520 ($^4A_2(F) \rightarrow {}^4T_1(P)$ triplet)	34
CoAPO-46	16 000; 17 150; 18 400 ($^4A_2(F) \rightarrow {}^4T_1(P)$ triplet); 20 800 ($^4T_{1g}(F) \rightarrow {}^4T_{2g}(F)$)	62
CoAPO-5	16 000; 17 300; 18 500 (tetrah coordination)	51
CoAPO-5	15 750; 17 240; 18 580 ($^4A_2(F) \rightarrow {}^4T_1(P)$ triplet)	63
$Cr_{0.01}APO\text{-}16(C)$	14 420 ($^4A_{2g} \rightarrow {}^2E_g$); 15 735 ($^4A_{2g} \rightarrow {}^4T_{2g}$); 22 380 ($^4A_{2g} \rightarrow {}^4T_{1g}(F)$)	this work
CrAPO-5	15 900 ($^4A_{2g} \rightarrow {}^4T_{2g}$); 21 800 ($^4A_{2g} \rightarrow {}^4T_{1g}(F)$)	20
CrAPO-5	16 130 ($^4A_{2g} \rightarrow {}^4T_{2g}$); 22 730 ($^4A_{2g} \rightarrow {}^4T_{1g}$)	64
CrAPSO-34	15 015; 17 390; 23 810	65
CrMCM-41	16 370 ($^4A_{2g} \rightarrow {}^4T_{2g}$); 21 410 ($^4A_{2g} \rightarrow {}^2T_{2g}$ (tetragonal distortion)); 22 470 ($^4A_{2g} \rightarrow {}^4T_{1g}$)	56
$Cr(H_2O)_6{}^{3+}$	15 000 ($^4A_{2g} \rightarrow {}^2E_g$); 17 400 ($^4A_{2g} \rightarrow {}^4T_{2g}$); 24 700 ($^4A_{2g} \rightarrow {}^4T_{1g}(F)$)	66
$Mn_{0.01}APO\text{-}16(C)$	15 870 (tetrah Mn^{2+}); 16 910 ($^6A_{1g} \rightarrow {}^4T_{1g}$); 20 430 (tetrah Mn^{2+}) 22 000 ($^6A_{1g} \rightarrow {}^4T_{2g}$); 23 490 (tetrah Mn^{2+}); 24 130 ($^6A_{1g} \rightarrow {}^4E_g, {}^4A_{1g}$); 24 400 (tetrah Mn^{2+})	this work
MnAPSO-34	18 870; 23 810; 25 000 (tetrah framework Mn^{2+})	65
MnO	16 400 ($^6A_1 \rightarrow {}^4T_2$); 20 800 ($^6A_1 \rightarrow {}^4T_2$); 23 800 ($^6A_1 \rightarrow {}^4E, {}^4A_1$)	67
$Mn(H_2O)_6{}^{2+}$	18 700 ($^6A_{1g} \rightarrow {}^4T_{1g}$); 23 120 ($^6A_{1g} \rightarrow {}^4T_{2g}$); 24 960 ($^6A_{1g} \rightarrow {}^4E_g, {}^4A_{1g}$)	66
$MnCl_4{}^{2-}$	21 250 ($^6A_1 \rightarrow {}^4T_1$); 22 235 ($^6A_1 \rightarrow {}^4T_2$); 23 020 ($^6A_1 \rightarrow {}^4E, {}^4A_1$)	66

associated with a local distortion of the cobalt sites. These spectral changes can be partially reversed by a hydrogen treatment at 623−673 K. This conclusion is supported by the recent work of Thomson et al.[70] for CoAPO-5. This group showed by DRS, ESR, and XANES−EXAFS that framework Co^{2+} ions are not oxidized, and this conclusion is in close agreement with recent ESR data on CoAPO-5, -11, -44 and -46 molecular sieves.[72] Indeed, Weckhuysen et al. reported that less than 30% of the ESR active Co^{2+} can be oxidized to Co^{3+} by a calcination treatment.[71]
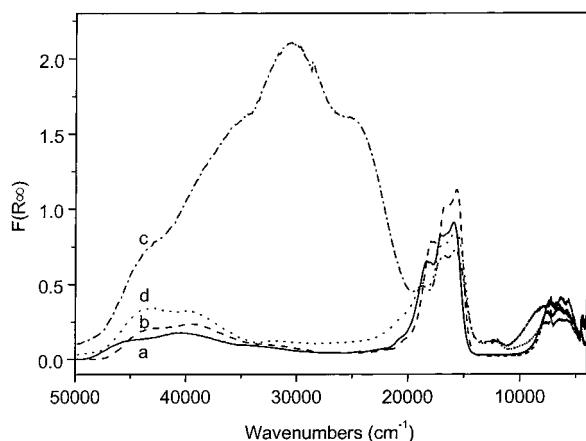
Transition Metal Ions in Molecular Sieves

J. Phys. Chem. B, Vol. 105, No. 14, 2001 **2685**

Figure 10. DRS spectra of $Co_{0.02}APO-16(C)$: (a) as-synthesized material, (b) after dehydration at 400 K, (c) after oxidation overnight at 873 K, and (d) after subsequent reduction in hydrogen at 623 K.

Conclusions

Transition metal ion-containing microporous aluminophosphates with AST structure either in the cubic or in the tetragonal form have been synthesized under hydrothermal conditions, and the materials were characterized by a portfolio of complementary characterization techniques. The following are the main conclusions from this work:

(1) Electronic spectroscopy reveals two distinct tetrahedrally coordinated Co^{2+} species in the AST structure. These two Co^{2+} species are most probably located in the two framework positions T_1 and T_2 with a T_1:T_2 occupation ratio of 3−8. Mn^{2+} can also be incorporated in the AST structure, although part of this ion is present as an extraframework octahedral species. V^{4+} and Cr^{3+} are not present as tetrahedrally coordinated framework species in the AST structure. Instead, V^{4+} is a highly dispersed pseudo-octahedrally coordinated species, which is strongly anchored onto the AST framework, while Cr^{3+} ions are present as octahedral species with some interaction with the framework. Both species can be considered as coordinated to defect lattice sites in the AST structure.

(2) The phase transition from the AST structure to the thermodynamically most stable berlinite structure can be considered as a criterion for the stability of the framework in the presence of transition metal ions. The observed sequence suggests that lower phase transition temperatures correspond to higher isomorphous substitution degrees of the transition metal ion. Thus, the degree of isomorphous substitution in the AST structure increases in the order $Cr \approx V < Mn < Co$. This is in line with spectroscopic observations.

(3) Transition metal ions, such as Co^{2+} and V^{4+}, are much more stable toward oxidative treatments in the AST structure than in other related microporous crystalline aluminophosphates.

References and Notes

(1) Flanigen, E. M.; Lok, B. M.; Patton, R. L.; Wilson, S. T. In *New Developments in Zeolite Science and Technology*; Murakami, Y., Iijima, A., Ward, J. W., Eds.; Kodansha: Tokyo, 1989; p 103.

(2) Wilson, S. T.; Flanigen, E. M. In *Zeolite Synthesis*; Ocelli, M. L., Robson, H. E., Eds.; ACS Symposium Series 398; American Chemical Society: Washington, DC, 1989; p 329.

(3) Hartmann, M.; Kevan, L. *Chem. Rev.* **1999**, *99*, 635.

(4) Weckhuysen, B. M.; Rao, R. R.; Martens, J. A.; Schoonheydt, R. A. *Eur. J. Inorg. Chem.* **1999**, 565.

(5) Verberckmoes, A. A.; Weckhuysen, B. M.; Schoonheydt, R. A. *Microporous Mesoporous Mater.* **1998**, *22*, 165.

(6) Goldfarb, D. *Zeolites* **1989**, *9*, 509.

(7) Katzmarzyk, A.; Ernst, S.; Weitkamp, J.; Knözinger, H. *Catal. Lett.* **1991**, *9*, 85.

(8) Levi, Z.; Raitsimring, A. M.; Goldfarb, D. *J. Phys. Chem.* **1991**, *95*, 7830.

(9) Brouet, G.; Chen, X.; Kevan, L. *J. Phys. Chem.* **1991**, *95*, 4928; Brouet, G.; Chen, X.; Lee, C. W.; Kevan, L., *J. Am. Chem. Soc.* **1992**, *114*, 3720.

(10) Finger, G.; Kornatowski, G.; Jancke, K.; Matschat, R.; Baur, W. H. *Microporous Mesoporous Mater.* **1999**, *33*, 127.

(11) Sinha, A. K.; Satyanarayana, C. V. V.; Srinivas, D.; Sivasanker, S.; Ratnasamy, P. *Microporous Mesoporous Mater.* **2000**, *35−36*, 471.

(12) Olender, Z.; Goldfarb, D.; Batista, J. *J. Am. Chem. Soc.* **1993**, *115*, 1106.

(13) Lohse, U.; Brückner, A.; Schreier, E.; Bertram, R.; Jaenchen, J.; Fricke, R. *Micropor. Mater.* **1996**, *7*, 139.

(14) Tusar, N. N.; Ristic, A.; Meden, A.; Kaucic, V. *Microporous Mesoporous Mater.* **2000**, *37*, 303.

(15) Arieli, D.; Vaughan, D. E. W.; Strohmaier, K. G.; Goldfarb, D. *J. Am. Chem. Soc.* **1999**, *121*, 6028.

(16) Chen, J. D.; Sheldon, R. A. *J. Catal.* **1995**, *153*, 1.

(17) Zhu, Z.; Wasowicz, T.; Kevan, L. *J. Phys. Chem.* **1997**, *101*, 10763.

(18) Prakash, A. M.; Hartmann, M.; Zhu, Z.; Kevan, L. *J. Phys. Chem.* **2000**, *104*, 1610.

(19) Eswaramoorty, M.; Jebarathinam, N. J.; Ulagappan, N. N.; Krinasamy, V. *Catal. Lett.* **1996**, *38*, 255.

(20) Weckhuysen, B. M.; Schoonheydt, R. A. *Zeolites* **1994**, *14*, 360.

(21) Weckhuysen, B. M.; Wachs, I. E.; Schoonheydt, R. A. *Chem. Rev.* **1996**, *96*, 3327.

(22) Rajic, N.; Stojakovic, D.; Hocevar, S.; Kaucic, V. *Zeolites* **1995**, *15*, 482.

(23) Demuth, D.; Unger, K. K.; Schuth, F.; Stucky, G. D.; Sdranov, V. I. *Adv. Mater.* **1994**, *6*, 931.

(24) Demuth, D.; Unger, K. K.; Schuth, F.; Sdranov, V. I.; Stucky, G. D. *J. Phys. Chem.* **1995**, *99*, 479.

(25) Prakash, A. M.; Kevan, L. *J. Phys. Chem. B.* **1999**, *103*, 2214.

(26) Wilson, S. T.; Lok, B. M.; Flanigen, E. M. *US Patent* 4, 310, 440, 1982.

(27) Schott-Darie, C.; Patarin, J.; Le Goff, P. Y.; Kessler, H.; Benazzi, E. *Micropor. Mater.* **1994**, *3*, 123.

(28) Schreyeck, L.; Caullet, P.; Mougenel, J. C.; Patarin, J.; Paillaud, J. L. *Micropor. Mater.* **1997**, *11*, 161.

(29) Lok, B. M.; Mesina, C. A.; Patton, R. L.; Gajek, R. T.; Cannan, T. R.; Flanigen, E. M. US Patent 4,440,871, 1986.

(30) Flanigen, E. M.; Lok, B. M.; Patton, R. L.; Wilson, S. T. EP Patent 158,976, 1985.

(31) Flanigen, E. M.; Lok, B. M.; Patton, R. L.; Wilson, S. T. US Patent 4,738,837, 1988.

(32) Wilson, S. T.; Lok, B. M.; Flanigen, E. M. US Patent 4,567,029, 1986.

(33) Kraushaar-Czarnetzki, B.; Hoogervorst, W. G. M.; Andrea, R. R.; Emeis, C. A.; Stork, W. H. J. In *Zeolite Chemistry and Catalysis*; Jacobs, P. A., et al., Eds.; Elsevier: Amsterdam, 1991; p 231.

(34) Kraushaar-Czarnetzki, B.; Hoogervorst, W. G. M.; Andrea, R. R.; Emeis, C. A.; Stork, W. H. J. *J. Chem. Soc., Faraday Trans* **1991**, *87*, 891.

(35) Bennett, J. M.; Kirchner, R. M. *Zeolites* **1991**, *11*, 502.

(36) Spectral optimization software provided by the Illinois ESR Research Center, NIH Division of research, grant RR01811. It includes the algorithm developed by K. J. Mattson, R. B. Clarkson, and R. L. Belford, (*11th International EPR Symposium*, *30th Rocky Mountain Conference*, Denver, Colorado, 1988) and generates a powder spectrum calculated to second order, for one metal nucleus with a spin $^1/_2$ or greater and three superhyperfine spins for which there can be more than one equivalent nucleus.

(37) The program is also provided by the Illinois ESR Research Center; it generates a powder spectrum for a spin $^1/_2$ or greater with one metal nucleus and superhyperfine spins. It allows also the introduction of zero-field splitting parameters, axial and rhombic.

(38) Frunza, L.; Van Der Voort, P.; Vansant, E. F.; Schoonheydt, R. A.; Weckhuysen, B. M. *Microporous Mesoporous Mater.* **2000**, *39*, 493.

(39) Balkus, K. J.; Gabrielov, A. G.; Shepelev, S. *Micropor. Mater.* **1995**, *3*, 489.

(40) Kornatowski, J.; Finger, G.; Jancke, K.; Richter-Mendau, J.; Schultze, D.; Joswig, W.; Baur, W. H. *J. Chem. Soc. Faraday Trans.* **1994**, *90*, 2141.

(41) Hartmann, M.; Azuma, N.; Kevan, L. *J. Phys. Chem.* **1995**, *99*, 10988.

(42) Flanigen, E. M.; Khatami, H.; Szimanski, H. A. In *ACS Symposium Series* 121; American Chemical Society: Washington, DC, 1971; p 201.

(43) Szostak, R.; Thomas, T. L. *J. Catal.* **1986**, *101*, 549.

(44) Peri, J. B. *Discuss. Faraday Soc.* **1971**, *52*, 55.

(45) Chen, J.; Thomas, J. M. *J. Chem. Soc. Chem. Commun.* **1994**, 603.

(46) Peeters, M. P. J.; van Hooff, J. H. C.; Sheldon, R. A.; Zholobenko, V. L.; Kustov, L. M.; Kazansky, V. B. In *Proceedings of the 9th International Zeolite Conference*; von Ballmoos, R., et al., Eds.; Butterworth: New York, 1993; p 654.

(47) Lourenco, J. P.; Ribeiro, M. F.; Ribeiro, R. F.; Rocha, J.; Onida, B.; Garrone, E.; Gabelica, Z. *Zeolites* **1997**, *18*, 398.

(48) Schrami-Marth, M.; Wokaun, A.; Pohl, M.; Krauss, H.-L. *J. Chem. Soc., Faraday Trans.* **1991**, *87*, 2617.

(49) Busca, G.; Ramis, G.; Lorenzelli, V. *J. Mol. Catal.* **1989**, *50*, 231.

(50) Weckhuysen, B. M.; Vannijvel, I. P.; Schoonheydt, R. A. *Zeolites* **1995**, *15*, 482.

(51) Montes, C.; Davies, M. E.; Murray, B.; Narayana, M. *J. Phys. Chem.* **1990**, *94*, 6431.

(52) Lohse, U.; Brückner, A.; Kinscher, K.; Parlitz, B. *J. Chem. Soc., Faraday Trans.* **1995**, *91*, 1173.

(53) Zahedi-Niaki, M. H.; Zaidi, S. M. J.; Kaliaguine, S. *Appl. Catal. A: General* **2000**, *196*, 9.

(54) Weckhuysen, B. M.; Schoonheydt, R. A.; Mabbs, F. E.; Collison, D. *J. Chem. Soc., Faraday Trans.* **1996**, *92*, 2431.

(55) Zhu, Z.; Kevan, L. *Phys. Chem. Chem. Phys.* **1999**, *1*, 199.

(56) Zhu, Z.; Chang, Z.; Kevan, L. *J. Phys. Chem.* **1999**, *103*, 2680.

(57) Akolekar, D.; Howe, R. F. *Stud. Surf. Sci. Catal.* **1997**, *105*, 755.

(58) Xu, J.; Luan, Z.; Wasowicz, T.; Kevan, L. *Microporous Mesoporous Mater.* **1998**, *22*, 179.

(59) De Vos, D. E.; Weckhuysen, B. M.; Bein, T. *J. Am. Chem. Soc.* **1996**, *118*, 9615.

(60) Davidson, A.; Che, M. *J. Phys. Chem.* **1992**, *96*, 9909.

(61) Ballhausen, C. J.; Gray, H. B. *Inorg. Chem.* **1992**, *1*, 111.

(62) Gao, Q.; Weckhuysen, B. M.; Schoonheydt, R. A. *Microporous Mesoporous Mater.* **1999**, *27*, 75.

(63) Sponer, J.; Cejka, J.; Dedecek, V.; Wichterlova, B. *Microporous Mesoporous Mater.* **2000**, 37, 117.

(64) Miyake, V.; Uehara, H.; Suzuki, H.; Yao, Z.; Matsuda, M.; Sato, M. *Microporous Mesoporous Mater.* **1999**, *32*, 45.

(65) Rajic, N.; Stojakovic, D.; Hocevar, S.; Kaucic, V. *Zeolites* **1993**, *13*, 384.

(66) Lever, A. B. P. *Inorganic Electronic Spectroscopy*, 2nd ed.; Elsevier: Amsterdam, 1984.

(67) Kijlstra, W. S.; Poels, E. K.; Bliek, A.; Weckhuysen, B. M.; Schoonheydt, R. A. *J. Phys. Chem.* **1997**, *101*, 309.

(68) Dyrek, K.; Che, M., *Chem. Rev.* **1997**, *97*, 305.

(69) Han, H. S.; Chon, H. *Microporous Mater.* **1994**, *3*, 331.

(70) Thomson, S.; Luca, V.; Howe, R. *Phys. Chem. Chem. Phys.* **1999**, *1*, 615.

(71) Weckhuysen, B. M.; Verberckmoes, A. A.; Uyttterhoeven, M. G.; Mabbs, F. E.; Collison, D.; de Boer, E.; Schoonheydt, R. A. *J. Phys. Chem. B* **2000**, *104*, 37.